Electron-impact excitation of the resonance transition in Ca^+

J. Mitroy,* D. C. Griffin,† and D. W. Norcross‡
Joint Institute for Laboratory Astrophysics, University of Colorado and National Bureau of Standards, Boulder, Colorado 80309-0440

M. S. Pindzola
Department of Physics, Auburn University, Auburn, Alabama 36489
(Received 7 March 1988)

Detailed calculations of the electron-impact excitation of Ca^+ are performed using both perturbation theory and the close-coupling approach. Particular attention is focused on the resonance ($4s$-$4p$) excitation since experimental emission-cross-section data are available for this transition. The results of the most sophisticated model, a six-state ($4s$, $3d$, $4p$, $5s$, $4d$, $5p$) close-coupling calculation with semiempirical Hartree-Fock target wave functions and including one- and two-body core-polarization potentials are in better agreement with the experimental cross section and resonance-fluorescence polarization data than any other calculation. At incident electron energies below the $5s$, $4d$, and $5p$ thresholds, the six-state calculations are essentially in agreement with the experimental data, although rich resonance structures predicted by theory are not seen experimentally due to the finite energy resolution. At energies above the $5s$, $4d$, and $5p$ thresholds the six-state emission cross sections exceed the experimental cross sections by about 20%, once allowance is made for cascades from the $5s$, $4d$, and $5p$ levels.

I. INTRODUCTION

In this paper we present the results of a detailed study of the electron-impact excitation of the resonance ($4s$-$4p$) transition of Ca^+. While the calculation of electron-ion cross sections is mainly motivated by the importance of cross-section information in a number of significant applications, e.g., the modeling of fusion and astrophysical plasmas, this was not the primary motivation for the present work. While many theoretical calculations of electron-ion collisions have been completed, experimental cross-section data are only available for relatively few ionic species. While it is not feasible to use experimental results to supply all the data needs of the fusion and astrophysical communities, these experimental studies play a pivotal role in testing the adequacy of the calculations. Comparison of experimental and theoretical cross-section data for a few selected ionic species can be used to provide an independent test of the accuracy of the theoretical techniques.

Most of the experimental studies to date have used photon emission techniques to determine the cross section. One of the best examples of a carefully done emission experiment is the work by Taylor and Dunn[1] on the excitation of the $4s$-$4p$ transition of Ca^+. Their choice of Ca^+ as a system to study was partly motivated by the relatively large number of published calculations[2–5] on this species at the time they initiated the experiment. Emission cross sections have also been measured by Zapesochnyi *et al.*[6] The results of this experiment confirm those of Taylor and Dunn. Zapesochnyi *et al.* also published emission cross sections for the excitation of the $5s$ and $4d$ levels from the ground state. Since excitations of the $5s$, $4d$, and $5p$ states result in cascades into the $4p$ state, the cross sections for these states are helpful in unraveling the emission cross sections of the $4p$ state. Somewhat paradoxically, while one would have expected that publication of experimental cross-section data would have stimulated further theoretical effort (especially in view of the fact that there were large discrepancies between theory and experiment), this has not been the case. Until very recently,[7] the only calculations[8–10] performed since the Taylor and Dunn experiment have been carried out using the distorted-wave approximation.

In this work we have undertaken some close-coupling calculations of the Ca^+ system at two different levels. Both three-state ($4s, 3d, 4p$) and six-state ($4s, 3d, 4p, 5s, 4d, 5p$) calculations have been performed. One- and two-body polarization potentials have been included at all stages of the calculations. In order to test the accuracy of the (unitarized) Coulomb-Born and distorted-wave approximations, we also report results for these approximations using exactly the same wave functions and polarization potentials. The remainder of this paper is arranged as follows. In Sec. II, we discuss the calculation of the Ca^+ bound-state wave functions, while in Sec. III we describe in detail the various levels of approximation used for the scattering calculations. The results of our calculations for the $4s$-$4p$ transition are presented in Sec. IV and compared with the results of other investigations. In Sec. V we describe the results of our calculations for the $4s$-$3d$ transition. In Sec. VI, we present cross sections for excitations to the $5s$, $4d$, and $5p$ levels from the ground state, and use them to estimate the cascade contribution to the $4p$ emission cross section. Finally, we summarize our results in Sec. VII and discuss their implications.

II. THE Ca^+ BOUND-STATE WAVE FUNCTIONS

We started this calculation with a very simple premise. A scattering calculation is only as accurate as the approximations for the target wave functions will allow. Therefore we have taken some care to ensure that our Ca^+ wave functions are as accurate as possible. A simplified model of the Ca^+ ion is to picture a loosely bound valence electron outside a tightly bound argonlike core. However, the $n=3$ core orbitals are not all that tightly bound [e.g., the Hartree-Fock (HF) eigenvalues are $\varepsilon_{3s}=-4.97$ Ry and $\varepsilon_{3p}=-3.16$ Ry]. As a consequence the Ca^{2+} core has a reasonable large dipole polarizability[11-13] ($\approx 3.2a_0^3$), large enough, in fact, to cause a significant perturbation of the valence-electron wave functions.

The effects of core polarization can be included in two distinctly different ways. One can use the *ab initio* approach, allowing virtual excitations from the $3s$ and $3p$ orbitals and constructing a configuration-interaction (CI) wave function. There are two problems with this approach that make it an unattractive method for a scattering calculation. First, using complicated CI wave functions to represent the Ca^+ bound states would greatly lengthen the time needed to do the calculations. Secondly, this approach does not include the core polarization effects "felt" by the second "scattered" electron. The alternative is to use the semiempirical approach. Initially we construct a set of fixed-core HF wave functions for the Ca^+ bound states. The semiempirical polarization potentials are then determined by the requirement that the calculated binding energies of the Ca^+ valence states by the same as the experimental binding energies. This approach has the advantages of being inexpensive to implement as well as providing a natural extension to the second "scattered" electron. For these reasons we adopted the semiempirical approach for this work.

In order to initiate our calculations we performed a series of numerical HF calculations (NHF) of the Ca^+ states using the Froese-Fischer[14] HF program. Koopman energies for the valence states determined from calculations using a relaxed core and fixed core (determined by calculations of the $4s$ state) are given in Table I. It is clear that the calculations using the $4s$ fixed core provide a reasonable approximation (except in the case of the $3d$ state) to the calculations with a relaxed core. Therefore the error introduced into the scattering calculation by the use of a fixed core is not expected to be large.

Analytic HF wave functions (AHF), however, were ultimately used for the scattering calculation. The primary reason for this is that the polarization potential has been included in our analytic HF program, while there is no provision for the inclusion of a polarization potential in the numerical HF program of Froese-Fischer. It is seen in Table I that the present Koopman energies calculated with a $4s$ fixed core are in excellent agreement with the numerical Koopman energies. Having adopted the $4s$ core, the description of the valence states is improved by including the semiempirical polarization potential in the Hamiltonian and recomputing the wave functions for the valence states. We choose a form for the polarization potential initially adopted by Norcross and Seaton:[16]

$$V_{\rm pol}(r)=\frac{-\alpha_d}{r^4}[1-\exp(-r^6/\rho_l^6)] \ . \tag{1}$$

The valence for the dipole polarizability (α_d) in the above expression was chosen[12,13] to be $3.16a_0^3$. The values of ρ_l in the expression are determined by the requirement that the computed binding energies of the $4s$, $4p$, $3d$, and $4f$ states be the same as the experimental binding energies (averaged for spin-orbit splitting). The values of ρ_l so determined were $1.6516a_0$, $1.6594a_0$, $1.9324a_0$, and $1.77a_0$, respectively, for $l=0$, 1, 2, and 3. The value of ρ_2 ($1.9324a_0$) seems anomalously large, primarily because the $3d$ orbital penetrates into the inner region of the atom much more than any other orbital and is thereby more sensitive to the polarization potential. The use of the polarization potential results in an immediate improvement which affects the scattering calculation. The binding energies of the semiempirical wave functions agree with the experimental binding energies to an accuracy of better than 1%. The HF binding energies, on the other hand, have an overall accuracy of about 5%. Since we use the same core potential for states with the same l value, the semiempirical wave functions were orthogonal to quite a high degree of precision; any residual nonorthogonality was removed by the Schmidt orthogonalization procedure.

TABLE I. Theoretical and experimental binding energies (in Ry) for the low-lying valence states of Ca^+. We use the abbreviations NHF and AHF to distinguish between calculations undertaken with the Froese-Fischer program and those done with the Slater-type orbital expansion technique.

State	NHF related core	NHF fixed $4s$ core	AHF fixed $4s$ core	AHF fixed $4s$ core + $V_{\rm pol}$	Expt.[a]
$4s$	−0.832 638	−0.832 638	−0.832 644	−0.872 556	−0.872 556
$3d$	−0.714 197	−0.675 276	−0.675 276	−0.747 836	−0.747 835
$4p$	−0.618 955	−0.619 631	−0.619 624	−0.641 642	−0.641 640
$5s$	−0.385 796	−0.386 260	−0.386 267	−0.396 064	−0.397 175
$4d$	−0.339 781	−0.339 982	−0.339 987	−0.350 302	−0.354 492
$5p$	−0.313 043	−0.313 354	−0.313 359	−0.320 132	−0.320 460
$4f$	−0.250 345	−0.250 377	−0.250 365	−0.252 376	−0.252 376

[a]Reference 15.

A further test of the quality of our wave functions lies in the calculation of the oscillator strengths between those states that will be included in the close-coupling expansion. A comparison of the absorption oscillator strengths, calculated at various levels of approximation are shown in Table II. Also shown in Table II are experimental oscillator strengths from a number of sources. In a number of instances, we used the published branching ratio[20] for transitions from $4p$ to $3d$ versus $4p$ to $4s$ to convert given values for the $4p$ lifetime into an oscillator strength. Focusing on the $4s$-$4p$ transition, it appears from the comparison between the HF and semiempirical oscillator strengths that the inclusion of the semiempirical polarization potential had a very small effect on the wave functions. However, this is only true superficially. The radial dipole integral, i.e.,

$$\langle r \rangle = \int_0^\infty dr\, P_{4s}(r) r P_{4p}(r) \tag{2}$$

is quite different for the two sets of wave functions. The value of this integral for the HF wave functions ($3.92a_0$) is larger than for the semiempirical wave functions ($3.78a_0$). The shrinking of the more tightly bound semiempirical wave functions, however, is counterbalanced in the calculation of the oscillator strength by the increased energy difference between the states.

More accurate values of the oscillator strengths require that a core-polarization correction be made to the dipole operator.[13,17,23] Oscillator strengths computed using a modified dipole operator,

$$\mathbf{r}' = \mathbf{r} - \frac{\alpha_d \hat{\mathbf{r}}}{r^2}[1 - \exp(-r^6/\bar{\rho}^6)]^{1/2} \tag{3}$$

are also given in Table II. The value of $\bar{\rho}$ used in this expression, namely, $1.75a_0$, was fixed by taking the average of ρ_0 through ρ_3. It should be mentioned that this correction is analogous to using the dielectronic polarization potential[16] in the scattering calculation. Again concentrating on the $4s$-$4p$ transition, we see that using a modified dipole operator results in a significantly smaller oscillator strength. This value for the oscillator strength is in agreement with the most precise of the experimental measurements, the Hanle effect experiment of Gallagher.[20] There is also reasonable agreement with the oscillator strength of Hafner and Schwartz.[17] This is to be expected since their calculation is conceptually similar to ours. The agreement with experiment for the other transitions is also uniformly good. [It should be mentioned that the present approach has been used to calculate oscillator strengths for Al^{2+}. There is excellent agreement (to within 0.5% for the $3s$-$3p$, $3s$-$4p$, $4s$-$3p$, and $4s$-$4p$ transitions) of the oscillator strengths calculated using the present approach with the accurate calculations of Froese-Fischer.[24]]

TABLE II. Comparison of absorption oscillator strengths calculated in a number of different approximations with experiment. We present oscillator strengths computed with both *ab initio* and semiempirical HF wave functions. The semiempirical oscillator strengths are also computed using a modified dipole-length operator with core-polarization correction. Theoretical values computed by Hafner and Schwartz (HS) (Ref. 17) and experimental values derived from a variety of sources are also presented.

	Ab initio HF		Semiempirical HF		Modified operator	HS	
Transition	f_l	f_v	f_l	f_v	f_l	f_l	Expt.
$4s$-$4p$	1.092	1.032	1.110	1.043	0.961	1.03	1.05±0.09[a] 1.02±0.1[b] 0.99±0.03[c] 0.90±0.08[d] 1.01±0.05[e]
$4s$-$5p$	$<10^{-4}$	0.0001	$<10^{-4}$	$<10^{-4}$	0.0019	$<10^{-4}$	
$4p$-$5s$	0.173	0.165	0.173	0.165	0.179	0.167	0.18±0.02[a] 0.16±0.02[d]
$5s$-$5p$	1.516	1.479	1.508	1.489	1.477	1.554	
$3d$-$4p$	0.049	0.0065	0.075	0.025	0.066	0.074	0.053±0.006[c]
$3d$-$5p$	0.0001	0.0005	0.0012	$<10^{-4}$	0.0004	0.0009	
$4p$-$4d$	0.865	0.800	0.900	0.837	0.869	0.794	0.87±0.09[a] 0.91±0.06[d] 0.82±0.05[d]
$4d$-$5p$	0.165	0.129	0.178	0.141	0.176	0.108	

[a]Reference 18.
[b]Reference 19.
[c]Reference 20.
[d]Reference 21.
[e]Reference 22.

III. DETAILS OF THE CALCULATION

We have performed a number of different calculations for the Ca^+ system. While these calculations often used quite different approaches, we have used exactly the same bound-state wave functions and Hamiltonian. Since the core-polarization potential was used in constructing the Ca^+ valence states, it was also included in the Hamiltonian for the second scattered electron for reasons of consistency. We made one minor change to the one-body part of the polarization potential felt by the "scattered" electron. A value of $1.7482a_0$ was adopted for ρ_2 because the value of $1.9324a_0$ obtained by fitting the $3d$ binding energy to experiment was thought to be anomalously large. If the binding energy of the $4d$ level is required to match with experiment then a value of $1.7482a_0$ is obtained. This value was thought to yield a more "typical" polarization potential for the $l=2$ partial wave of the scattering electron. Note that a value of $1.77a_0$ was uniformly adopted for $l \geq 3$.

The two-body dielectronic polarization potential was also included in the Hamiltonian. The form adopted for this potential was

$$V_{\rm diel}(r_1,r_2) = -2\alpha_d \frac{\hat{\mathbf{r}}_1\cdot\hat{\mathbf{r}}_2}{r_1^2 r_2^2}\{[1-\exp(-r_1^6/\bar{\rho}^6)] \times [1-\exp(-r_2^6/\bar{\rho}^6)]\}^{1/2} . \quad (4)$$

The value adopted for $\bar{\rho}$, i.e., $1.75a_0$, was the same as that used in Eq. (3).

The different calculations are now described in order of increasing complexity.

(i) UCBAV6. This was a fully unitarized Coulomb-Born calculation (with exchange up to a total angular momentum of 10) with on-shell coupling included between six states ($4s$, $3d$, $4p$, $5s$, $4d$, and $5p$).

(ii) UDWV6. This was a fully unitarized distorted-wave calculation (with exchange) with on-shell coupling included between six states ($4s$, $3d$, $4p$, $5s$, $4d$, and $5p$). The distorted waves were computed in the exact static-exchange potential appropriate for each channel.

(iii) CC3. This was the only calculation in which we did *not* include polarization potentials. Three states ($4s, 3d, 4p$) were explicitly coupled in the close-coupling approximation. These states were represented by fixed-core *ab initio* HF wave functions and the polarization potentials were omitted. Exchange was included up to a total angular momentum of 10.

(iv) CCV3. This calculation is the same as the CC3 calculation except that semiempirical wave functions were used and the one- and two-body polarization potentials were included in the scattering Hamiltonian.

(v) CCV6. This calculation was the same as the CCV3 calculation except that six states ($4s$, $3d$, $4p$, $5s$, $4d$, and $5p$) were explicitly coupled together in the close-coupling expansion. To properly map the resonance structure for the $3d$ and $4p$ excitations at incident energies below the $5p$ threshold, a very fine energy mesh (0.01 Ry) was used in this energy range.

The angular algebra for the close-coupling calculations described above were performed using COLALG (Ref. 25) and CCALG.[26] The numerical solutions of the coupled radial equations were determined using IMPACT.[27] The IMPACT calculations were carried out at two different sites using two different versions of the programs. Since the lowest three states of the Ca^+ ion are energetically quite close, one would expect that coupling effects would remain strong, even for quite high partial waves. We used IMPACT to solve the CC equations up to a maximum value of the total angular momentum L of 20. In order to have sufficient accuracy in the solutions for high values of L, it was necessary to use different radial integration meshes for the different partial waves. For low values of L, a rather fine mesh was used. However, for higher partial waves, where the centrifugal barrier causes the first inflection point in the radial wave function to occur at relatively large values of r, the starting region, which is represented by a power series, needed to be extended. Therefore, for $L \geq 7$, we increased the number of points in the starting region from 5 to 9. However, in order to keep the number of tabular points to a reasonable size, we also increased the distance between mesh points as follows. With the first mesh point equal to zero, the second mesh point is given by $r_2 = \nabla_1/Z$,[27] where Z is the nuclear charge. For $L < 7$, ∇_1 was set to 0.1, while for $L \geq 7$, it was increased to 0.3.

Nevertheless, except for the lower energies, it was not possible to include enough partial waves with IMPACT to get converged cross sections for the $4s$-$3d$ and $4s$-$4p$ transitions. Different techniques were used to take into account the contributions from the higher partial waves. In the first method, we supplemented the IMPACT K matrices with K matrices for high values of L calculated in the unitarized Coulomb-Born approximation. Three-state Coulomb-Born K matrices were used for the CCV3 calculations and six-state Coulomb-Born calculations were used for the CCV6 calculations. The maximum L value for which Coulomb-Born calculations were performed was increased with energy, and for the highest energy of 2.0 Ry, we added Coulomb-Born contributions up to $L=60$ to the IMPACT results.

The second method by which the partial-wave sum was completed exploited the fact that, for sufficiently high partial waves, the partial cross sections form a geometric series.[2] If there exists a value of L, e.g., L_0, such that for $L \geq L_0$,

$$\frac{Q_L}{Q_{L-1}} = \text{const} = x , \quad (5)$$

then the sum of partial cross sections to infinity can be performed analytically by

$$\sum_{L=L_0}^{\infty} Q_L = Q_{L_0}/(1-x) . \quad (6)$$

In general, sufficiently many partial waves were computed with the IMPACT program to ensure the potential error involved was minimized.

Finally, for optically allowed transitions, Burgess[28] has derived a sum rule based on the Coulomb-Bethe approxi-

mation. Recently, Burke and Seaton[29] described the use of this method in conjunction with close-coupling calculations, and for comparison with the other two methods, we also completed the partial-wave sum for the $4s$-$4p$ transition using this form of the Burgess sum rule.

IV. EXCITATION OF THE RESONANCE TRANSITION

Total cross sections for the Ca^+ $4s$-$4p$ transition are given in Table III for a large variety of different theoretical approaches. We have taken the liberty of interpolating previously published cross section data for presentation in Table III. One feature is immediately apparent from even a cursory glance. All of the present calculations which use polarization potentials and semiempirical wave functions (i.e., excluding the CC3 results) yield lower total cross sections than any of the previous calculations. The comparison of CC3 and CCV3 results provides a dramatic illustration of the importance of including the polarization potentials. The CCV3 cross sections are some 20% lower at all energies at which a comparison has been made. It is readily apparent that this is not a feature that is peculiar to the present calculations; the three-state close-coupling calculations of Burke and Moores[2] give cross sections which agree reasonably well with the CC3 results and are also much larger than the CCV3 results.

A pleasing feature of Table III is that all techniques for completing the partial-wave sum for the CCV6 calculations yield very close results for the total cross sections. Only at the highest energy, where the partial waves above $L=20$ add from 16% to 17% to the total cross section, are the differences of any significance. The larger discrepancy between CCV6 and CCV6** could be due to coupling effects which are not included in the Burgess sum rule, as well as to the inclusion of only the long-range part of the interaction between the continuum and valence electrons in deriving the Burgess sum rule from the Bethe approximation. Finally, in order to test the completeness of the partial-wave sum up to $L=60$ in CCV6 at 2.0 Ry, we employed the Burgess sum rule to complete the sum from $L=61$ to ∞, and found that it added only $0.02\pi a_0^2$ to the total cross section.

Comparison of the perturbation theory results, i.e., the UCBAV6 and UDWV6 cross sections, with each other and with the CCV6 results, reveals that these conceptually simple and computationally inexpensive approximations do a surprisingly good job of reproducing the close-coupling calculations. At the highest energy considered, the UCBAV6, UDWV6, and CCV6 cross sections differ by less than 2%. Even at the lowest energy, just above the $4p$ threshold, the UCBAV6 and UDWV6 cross sections exceed the CCV6 cross section by less than 20% and because they include polarization effects are smaller than the close-coupling calculation of Burke and Moores.

A detailed look at the individual partial cross sections at incident energies of 1.0 and 2.0 Ry (Table IV) provides further insight into the comparison between perturbation theory and the close-coupling approach. One fact is immediately obvious—the good agreement between the UCBAV6 and UDWV6 partial cross sections for the higher partial waves indicates that distortion is relatively unimportant in this region. This is to be expected since

TABLE III. Comparison of total cross sections (in units of πa_0^2) for the $4s$-$4p$ transition in Ca^+ computed in a variety of different approaches. The* is used to denote close-coupling calculations for which the partial-wave sum was completed using the power-series extrapolation technique. The** is used to denote close-coupling calculations for which the partial-wave sum was completed using the Burgess sum rule. (The calculations without an asterisk used the unitarized Coulomb-Born approximation to complete the partial-wave sum.)

	Energy (Ry)						
	0.25	0.35	0.50	0.70	1.00	1.40	2.00
CDWII[a]	68.4	62.4	41.4		37.5		24.4
CBOII[b]	64.3	58.2	50.1		37.5		28.7
DWPOII[c]	49.5	46.4	42.0		33.4		24.1
CBII[d]	44.3	42.3	39.2		31.7		21.7
CDWII2[e]	43.6	44.2	42.4		34.2		23.8
BM[f]	39.95	41.34	40.98	38.91	35.47		
UCBAV6	37.46	37.12	34.94	29.44	26.20	22.95	19.47
UDWV6	37.94	37.72	35.44	29.84	26.71	23.49	19.69
CC3*	37.13	39.64	39.77	38.25	35.47		
CCV3	30.82	32.23	31.80	30.13	27.37	24.17	20.47
CCV6	31.52	31.38	27.63	25.64	24.42	22.20	19.27
CCV6*	31.50	31.38	27.63	25.64	24.42	22.18	19.20
CCV6**	31.50	31.38	27.63	25.64	24.41	22.15	19.11

[a]Unitarized distorted-wave calculation, Ref. 8.
[b]Unitarized Coulomb-Born-Oppenheimer calculation, Ref. 9.
[c]Unitarized distorted-wave polarized-orbital calculation, Ref. 9.
[d]Unitarized Coulomb-Born calculation, Ref. 10.
[e]Unitarized distorted-wave calculation, Ref. 10.
[f]Three-state close-coupling calculation, Ref. 2.

TABLE IV. Comparison of partial cross sections (in units of πa_0^2) for the $4s$-$4p$ transition at incident electron energies of 1.0 and 2.0 Ry.

	$E=1.0$ Ry				$E=2.0$ Ry			
L	CCV3	UCBAV6	UDWV6	CCV6	CCV3	UCBAV6	UDWV6	CCV6
0	0.035	0.229	0.038	0.032	0.039	0.103	0.027	0.035
1	0.609	0.365	0.568	0.506	0.177	0.046	0.182	0.167
2	0.925	0.356	0.917	0.780	0.577	0.071	0.548	0.521
3	1.344	0.874	1.473	1.156	0.529	0.181	0.527	0.492
4	2.452	2.795	2.497	2.040	0.483	0.790	0.486	0.453
5	3.729	3.528	3.455	3.340	1.190	1.274	1.176	1.093
6	3.629	3.379	3.282	3.155	1.520	1.522	1.478	1.458
7	3.166	2.958	2.898	2.686	1.686	1.570	1.543	1.543
8	2.540	2.488	2.457	2.229	1.617	1.502	1.484	1.475
9	2.008	2.033	2.011	1.822	1.474	1.386	1.372	1.341
10	1.571	1.623	1.605	1.467	1.321	1.258	1.251	1.214
11	1.222	1.275	1.259	1.162	1.171	1.130	1.122	1.080
12	0.946	0.991	0.978	0.912	1.034	1.010	1.001	0.962
13	0.731	0.766	0.757	0.712	0.910	0.899	0.890	0.853
14	0.564	0.590	0.583	0.553	0.801	0.797	0.788	0.758
15	0.435	0.453	0.449	0.428	0.704	0.705	0.697	0.671
16	0.335	0.348	0.344	0.331	0.619	0.623	0.615	0.593
17	0.258	0.267	0.265	0.255	0.544	0.549	0.542	0.525
18	0.198	0.205	0.203	0.196	0.478	0.484	0.477	0.464
19		0.157	0.156	0.151		0.427	0.420	0.409
20		0.121	0.120	0.116		0.376	0.369	0.362

the incident energies are not sufficiently large in either case for the incident electron to penetrate into the centripetal barrier at large L values. However, there are large differences between the UCBAV6 and UDWV6 partial cross sections at lower L values. The UDWV6 cross sections are in much better agreement with the CCV6 cross sections, indicating that the inclusion of distortion is important here. Therefore, not too much significance should be attached to the fact that the UCBAV6 total cross section is generally in better agreement with the CCV6 cross section than the UDWV6. The UCBAV6 calculation is lower than the CCV6 cross sections at low L values, this partially compensates for the error made for larger L values where the UCBAV6 calculation overestimates the partial cross sections.

A comparison of the present calculations with the experimental $4p_{3/2}$ emission cross section data of Refs. 1 and 6 is depicted in Figs. 1 and 2. The error limits (roughly 10%) of Taylor and Dunn are at the 98% confidence level. Taylor and Dunn also measured emission cross sections for the $4p_{1/2}$-$4s$ transition. They found the ratio of the $4p_{3/2}$:$4p_{1/2}$ emission cross sections to be equal to 2.0 within experimental error. The emission data of Zapesochnyi *et al.* have much larger absolute errors. There is an overall calibration uncertainty of 16% and a statistical error of about 4%. Furthermore, the data of Zapesochnyi *et al.* that we depict have not been corrected for anisotropy effects that result from the fact that the fluorescence radiation is polarized. Two figures are used for the comparison in order to resolve the resonance structure below the $5s$, $4d$, and $5p$ thresholds. Since Figs. 1 and 2 depict emission cross section data for only the K line (i.e., $4p_{3/2}$-$4s$) it is necessary to multiply the calculated $4p$ multiplet cross sections by a factor of $\frac{2}{3}$. A further multiplicative factor of 0.946 comes from the fact that the $4p_{3/2}$ level can also decay into the $3d$ metastable state as well as the ground state with a ratio of radiative rates[20] of 1:17.6.

At incident electron energies below the $5s$, $4d$, and $5p$ excitation thresholds the CCV6 calculation is in good

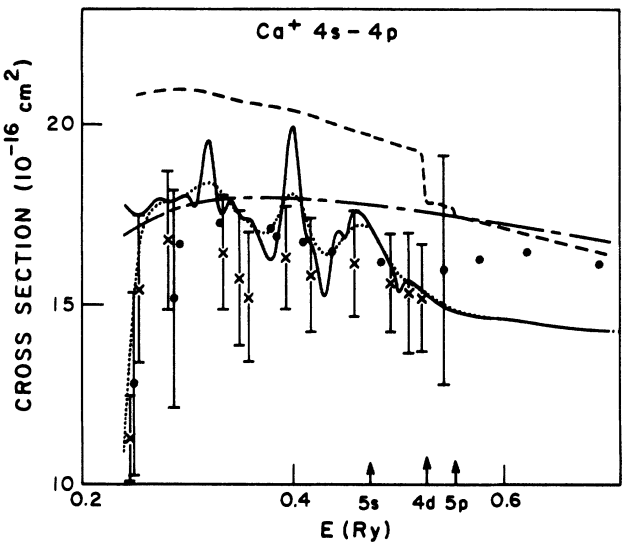

FIG. 1. Absolute emission cross section (in 10^{-16} cm^2) for electron-impact excitation of the Ca^+ $4p_{3/2}$ state as a function of incident energy (in Ry). The following calculations are depicted: CCV6 (——), CCV3 (– – –), UCBAV6 (— — —), and the CCV6 convoluted with an energy resolution function of full width 0.023 Ry (· · · ·). The experimental data of Refs. 1 and 6 are depicted as × and ●, respectively.

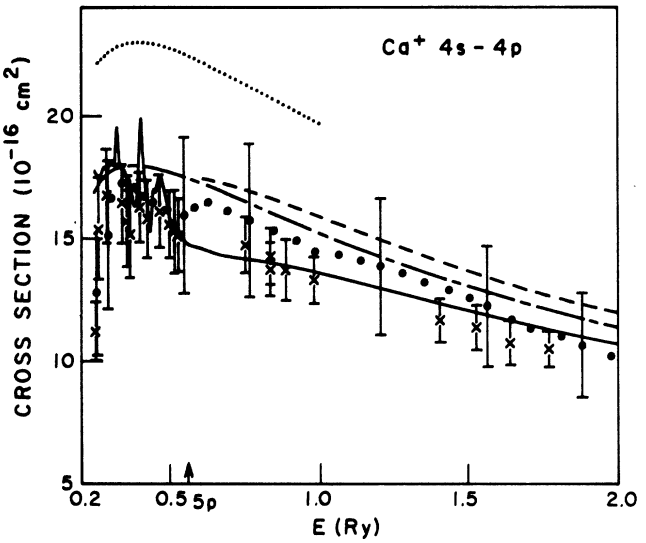

FIG. 2. Absolute emission cross section (in 10^{-16} cm^2) for electron-impact excitation of the Ca^+ $4p_{3/2}$ state as a function of incident energy (in Ry). The following calculations are depicted: CCV6 (——), CCV3 (— - — -), the CCV6 cross section with cascade corrections (— — —), and the three-state close-coupling calculations (· · · ·) of Ref. 2. The experimental data of Refs. 1 and 6 are depicted as × and ●, respectively.

agreement with experiment. The experimental energy resolution (0.023 Ry in the experiment of Taylor and Dunn) precludes a detailed comparison with the resonances, although the data of Ref. 1 do show signs of structure which are consistent with the CCV6 results. To demonstrate the effect that finite-energy resolution will have on the experiment we have convoluted the CCV6 calculation with a normal probability distribution of full width 0.023 Ry and plotted the results in Fig. 1. The resonance structure of the convoluted cross section has been greatly smoothed. The remaining fluctuations are roughly the same size as the fluctuations of Taylor and Dunn, and moreover the positions of the peaks and valleys of the convoluted cross section seem to be consistent with those seen experimentally. The convoluted cross section also does a good job of reproducing the gradual decrease of the experimental cross section at threshold. The CCV3 cross section naturally shows no sign of any resonance structure and generally exceeds the cross section data of Taylor and Dunn in the low-energy region. The error limits of Ref. 6 are too large to discriminate between the accuracy of the CCV3 and CCV6 calculations. At incident energies above the $5p$ threshold the CCV6 calculation gives smaller cross sections than the CCV3 calculation, once again in good agreement with the experiment of Taylor and Dunn. However, cascades from excitations to the $5s$, $4d$, and $5p$ levels will have an influence on the emission cross section in this region. A detailed discussion of this effect is postponed until Sec. VI.

A further test of these calculations can be made by examining the polarization of the radiation emitted in the decay of the $4p$ state. It is possible to resolve the radiation emitted by the $4p_{3/2}$ and $4p_{1/2}$ states. Radiation emitted by the $4p_{1/2}$ state is isotropic and will not be considered further. Since 99.85% of the Ca isotopes have zero nuclear spin[2] the percentage polarization of the $4p_{3/2}$-$4s_{1/2}$ decay is given by[30]

$$P = 300(Q_0 - Q_1)/(5Q_0 + 7Q_1) . \quad (7)$$

In this expression Q_0 is the cross section for exciting the $4p$ $M=0$ substate and Q_1 is the cross section for exciting the $M=1$ substate.

Saraph[31] used the K matrices computed by Burke and Moores[2] to first compute the polarization of the $4p$-$4s$ decay. Unfortunately, an expression for the scattering amplitude which omitted the Coulomb phase[32] was used to compute the excitation cross sections of the different magnetic sublevels. Since it is not possible to evaluate what effect this omission would have had on the polarization we do not make any comparison with these results.

Values for the polarization computed in the UCBAV6, CCV3, and CCV6 models are compared with each other and with experiment in Figs. 3 and 4. The use of this unitarized Coulomb-Born approximation was an essential element in the evaluation of Q_0 and Q_1, as the Burgess sum rule is inapplicable. It is clear that the most sophisticated calculation (i.e., the CCV6 model) provides the best agreement with experiment at nearly all energies. At threshold, the CCV6 calculation predicts a lower value of the polarization than the CCV3 calculation, in better agreement with experiment. At higher energies the CCV6 calculation gives a larger value of the polarization than the CCV3 calculation, again in better accord with experiment. The UCBAV6 calculation does a uniformly poor job of reproducing the experimental polarization. This is perhaps a consequence of the poor job the

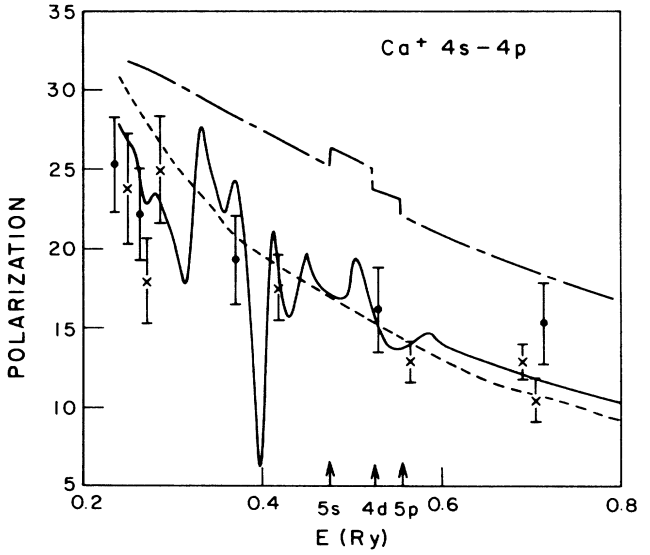

FIG. 3. Percentage linear polarization of the Ca^+ $4P_{3/2}$-$4s$ fluorescence radiation emitted perpendicular to the scattering plane as a function of incident energy (in Ry). The following calculations are depicted: CCV6 (——), CCV3 (— — —), and UCBAV6 (— - — -). The experimental data of Refs. 1 and 6 are depicted as × and ●, respectively.

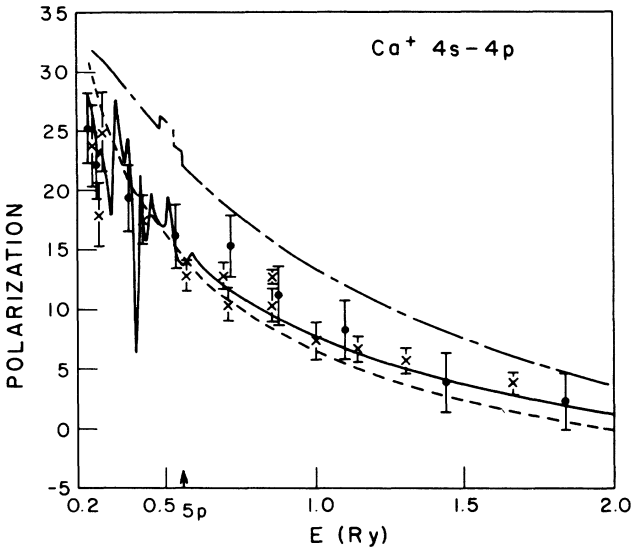

FIG. 4. Percentage linear polarization of the Ca^+ $4p_{3/2}$-4s fluorescence radiation emitted perpendicular to the scattering plane as a function of incident energy (in Ry). The following calculations are depicted: CCV6 (——), CCV3 (— — —), and UCBAV6 (—·—·). The experimental data of Refs. 1 and 6 are depicted as × and ●, respectively.

UCBAV6 calculation does of modeling of low partial waves. One of the interesting features of the CCV6 calculation seen in Fig. 3 is the strong resonance structure seen below the 5s, 4d, and 5p thresholds. It is somewhat unfortunate that no experimental data points were taken sufficiently close to the deep minimum at 0.4-Ry incident energy.

V. EXCITATION OF THE 3d STATE

Since the 3d level is located within 2 eV of both the 4s and 4p levels, almost midway between them, we would intuitively expect that the 3d state will couple strongly with both of these levels. There are two dominant reaction mechanisms for exciting the 3d state. One can have a direct excitation of the 3d state via the quadrupole interaction coupling it with the 4s ground state. Alternatively, it is possible to conceive of a two-step process involving the coupling of the 4s state to the 4p state which then couples to the 3d state.

Comparisons of 3d cross sections computed in a number of different approximations are given in Table V. Unlike the situation for the 4p excitation, the UCBVA6 and UDWV6 calculations do not do a very good job of reproducing the CCV6 calculation. For example, at an incident energy of 0.25 Ry the UCBAV6 calculation exceeds the CCV6 result by a factor of 2.5 while the UDWV6 cross section is 50% larger. At the highest incident energy considered, the UCBAV6, and UDWV6 models are in much closer agreement with the six-state close-coupling results, although differences of 7–11% remain.

The excitation cross section for the 3d state is depicted in Fig. 5. Very strong resonance structures occur below the 5s and 4p thresholds. Below the 4p threshold the resonances would cause a considerable increase in an energy-averaged 3d cross section. Indeed the maximum value of the 3d cross section, achieved at an incident energy of 0.17 Ry, is about twice the size of maximum value attained for the dipole-allowed 4p transition.

Further examples of the inadequacy of perturbation theory for this transition are seen in the comparison of the individual partial cross sections given in Table VI. There is poor agreement between the UCBAV6 and UDWV6 calculations at small L values. As expected the differences essentially disappear at larger values of L. However, there are large differences between the perturbation theory and close-coupling cross sections for almost all L values. The most notable feature of this is the fact that the UCBAV6 cross sections are still twice as large as the CCV6 cross sections at $L=20$. This emphasizes the strength of off-shell coupling effects for this transition.

Detailed comparisons of the partial cross sections for the CCV6 calculation reveals that the ratio, Q_L/Q_{L-1} is still increasing slowly at $L=20$ for energies above 0.9 Ry. Therefore the power series extrapolation, Eq. (6), should

TABLE V. Comparison of total cross sections (in units of πa_0^2) for the Ca^+ 4s-3d transition computed in a variety of approximations. (The calculations without an asterisk used the unitarized Coulomb-Born approximation to complete the partial-wave sum.)

	Energy (Ry)							
	0.15	0.25	0.35	0.50	0.70	1.00	1.40	2.00
CBII[a]		10.9	9.09	5.60	4.03	2.77		1.41
CDWII2[b]		10.05	8.67	6.78	5.02	3.48		1.68
BM[c]		12.90	8.39	5.37	3.63	2.54		
UCBAV6	32.94	21.86	14.04	8.28	4.86	2.89	1.87	1.26
UDWV6	22.51	12.94	8.97	5.99	3.77	2.48	1.76	1.26
CC3*		14.56	9.48	6.02	4.09	2.86		
CCV3	18.52	10.44	6.75	4.34	3.02	2.19	1.66	1.23
CCV6	17.78	8.50	6.07	4.48	2.57	1.96	1.55	1.18
CCV6*	17.78	8.51	6.08	4.48	2.59	1.95	1.52	1.14

[a]Unitarized Coulomb-Born calculation, Ref. 10.
[b]Unitarized distorted-wave calculation, Ref. 10.
[c]Three-state close-coupling calculation, Ref. 2.

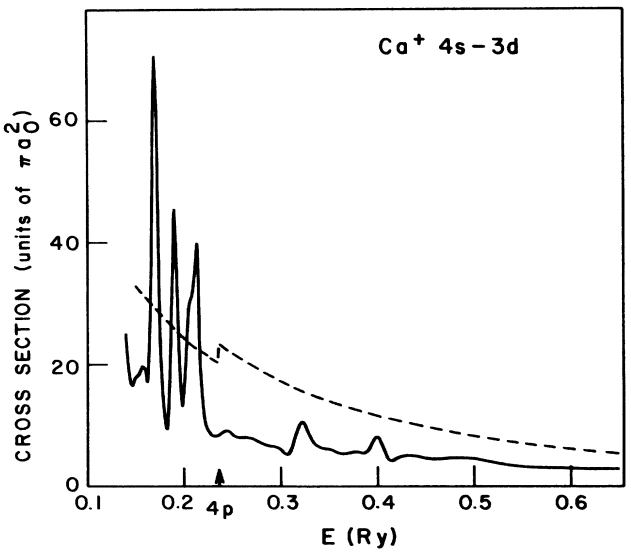

FIG. 5. Total cross sections (in units of πa_0^2) for excitation of the Ca^+ 4*s*-3*d* transition as a function of the incident energy (in Ry). The CCV6 (——) and UCBAV6 (— — —) calculations are depicted.

underestimate the actual cross section at these energies. Since the use of the UCBAV6 cross sections will obviously overestimate the contribution from the high partial waves, these two different means of accounting for the higher partial waves should provide a lower and upper bound to the true cross section. Values of the total 4*s*-3*d* excitation cross section obtained by these two methods are in reasonable agreement. The largest difference between the two methods occurs at an incident energy of 2.0 Ry and is only 4%.

VI. CASCADE CORRECTIONS TO THE 4*p* EMISSION CROSS SECTION

Since the experimental 4*p* cross sections come from an emission experiment it is possible, and indeed quite likely, that the results could be affected by cascades from excitations of higher levels. For instance, excitations of the 5*s*, 4*d*, and 5*p* levels from the ground state will result in cascades into the 4*p* state, thus causing the effective emission cross section to exceed the actual 4*p* cross section. In this section we report cross sections for exciting the 5*s*, 4*d*, and 5*p* states in order to get some estimate of the cascade correction.

Cross sections for the 5*s* state are given in Table VII. It can be seen that the differences between the CCV6, UCBAV6, and UDWV6 calculations are relatively large. This is not surprising since this is monopole transition with a relatively large excitation energy. Hence the dominant contributions to the cross section will come from the low partial waves where both distortion and coupling effects are quite substantial.

Total cross sections for exciting the 4*d* state are given in Table VII. The excitation cross sections for this state are relatively large. At threshold the 4*d* cross section is about 15% the size of the 4*p* cross section and is actually larger than the 4*s*-3*d* cross section.[7] The agreement between the UCBAV6, UDWV6, and CCV6 cross sections improves with increasing energy and the spread between the three calculations is only 10% at 2.0 Ry.

Emission cross sections for excitation of both the 5*s* and 4*d* states are given in Ref. 6. The fluorescence radia-

TABLE VI. Comparison of partial cross section (in units of πa_0^2) for the 4*s*-3*d* transition at an incident energies of 1.0 and 2.0 Ry.

	$E=1.0$ Ry				$E=2.0$ Ry			
L	CCV3	UCBAV6	UDWV6	CCV6	CCV3	UCBAV6	UDWV6	CCV6
0	0.025	0.021	0.040	0.025	0.007	0.014	0.014	0.007
1	0.185	0.160	0.117	0.165	0.037	0.090	0.038	0.038
2	0.262	0.631	0.264	0.258	0.088	0.058	0.063	0.090
3	0.331	0.536	0.482	0.318	0.130	0.153	0.168	0.127
4	0.607	0.393	0.397	0.466	0.251	0.152	0.178	0.233
5	0.286	0.271	0.283	0.279	0.162	0.138	0.142	0.167
6	0.164	0.210	0.215	0.149	0.131	0.121	0.122	0.123
7	0.094	0.159	0.165	0.086	0.098	0.102	0.105	0.092
8	0.055	0.117	0.121	0.051	0.070	0.082	0.085	0.066
9	0.034	0.086	0.088	0.032	0.049	0.065	0.067	0.047
10	0.022	0.063	0.065	0.022	0.035	0.050	0.052	0.034
11	0.016	0.048	0.049	0.015	0.025	0.039	0.040	0.024
12	0.012	0.037	0.037	0.012	0.019	0.031	0.032	0.018
13	0.009	0.029	0.029	0.009	0.014	0.025	0.025	0.014
14	0.008	0.023	0.023	0.007	0.011	0.020	0.020	0.011
15	0.006	0.018	0.018	0.006	0.008	0.016	0.017	0.008
16	0.005	0.015	0.015	0.005	0.007	0.014	0.014	0.007
17	0.005	0.012	0.012	0.005	0.006	0.011	0.011	0.005
18	0.004	0.010	0.010	0.004	0.005	0.009	0.010	0.005
19		0.009	0.009	0.004		0.008	0.008	0.004
20		0.007	0.007	0.003		0.007	0.007	0.003

TABLE VII. Total excitation cross sections (in units of πa_0^2) for electron-impact excitation of the Ca^+ 5s, 4d, and 5p states from the ground state.

	Energy (Ry)						
	0.6	0.8	1.0	1.2	1.4	1.7	2.0
				5s			
UCBAV6	0.883	0.656	0.527	0.453	0.407	0.360	0.328
UDWV6	1.10	0.879	0.761	0.690	0.642	0.588	0.543
CCV6	1.37	1.19	0.993	0.867	0.785	0.669	0.634
				4d			
UCBAV6	2.59	2.35	2.07	1.83	1.64	1.41	1.22
UDWBV	2.23	2.51	2.20	1.96	1.74	1.48	1.30
CCV6	3.35	3.18	2.65	2.23	1.92	1.59	1.36
				5p			
UCBAV6	0.593	0.587	0.499	0.418	0.360	0.298	0.257
UDWV6	0.782	0.712	0.660	0.593	0.529	0.446	0.379
CCV6	0.479	0.524	0.506	0.481	0.448	0.395	0.347

tion for decay into the $4p_{3/2}$ level has been measured for both of these transitions. A comparison of the experimental emission cross sections with calculated emission cross sections is shown in Fig. 6. To convert the calculated excitation cross sections for the 5s and 4d levels into the appropriate emission cross sections we have multiplied by the factor $\frac{2}{3}$. While the CCV6 calculation agrees with the 5s emission cross section, it is about a factor of 4 times larger than the 4d emission cross section.

Excitations into the 5p state do not result in direct cascade into the 4p state. The 5p state must first decay into either the 4d or 5s states, which then feed into the 4p state. However, the 5p state can also decay directly into the 3d or 4s states. We have determined the branching ratio for the 5p state to cascade into the 4p state by converting the oscillator strengths given in Table II into transition rates. We find that an excitation of the 5p level will eventually decay into the 4p state 91% of the time. Using this number we can now write down an expression for the effective emission cross section of the $4p_{3/2}$ state:

$$Q_{\rm em}=2\times 0.946(Q_{4p}+Q_{5s}+Q_{4d}+0.91Q_{5p})/3 \ . \quad (8)$$

A comparison of the effective emission cross section, Eq. (8), with the experimental data is given in Fig. 2. Adding the cascade corrections to the $4p_{3/2}$ cross section results in a 20% increase in the emission cross section just above the 5p threshold. At the highest energy (2.0 Ry) cascades cause a 12% increase in the cross section. It is clear from Fig. 2 that the inclusion of cascade corrections results in a significant degradation of the agreement between the CCV6 calculation and experiment.

Although another recent six-state close-coupling calculation[7] also suggests a cascade correction of roughly 20% near the 5p threshold, the available experimental evidence indicates that CCV6 calculation overestimates the cascade contribution. There is a small increase in the emission cross section of Zapesochnyi *et al.* in the threshold region of the 5s, 4d, and 5p states. However, the size of the increase in the cross section is a factor of 2 smaller than the calculated increase due to cascades. The cross section data of Taylor and Dunn show no indication of an appreciable cascade contribution to the emission cross section. The absence of any significant structure in the resonance emission cross section at the 5s and 4d thresholds (see Fig. 9 of Ref. 1) suggests that the combined cascade contribution from these two levels is probably less than 5%. Finally, the dominant contribution to the calculated cross section comes from the decay of the 4d state. The direct comparison of the calculated and measured cross sections shown in Fig. 6 suggests that this contribution may be greatly overestimated.

Although our final result, with the cascade correction, overestimates the $4p_{3/2}$ emission cross section above the 5p threshold it is possible that a larger calculation, with coupling between more states, will result in better agree-

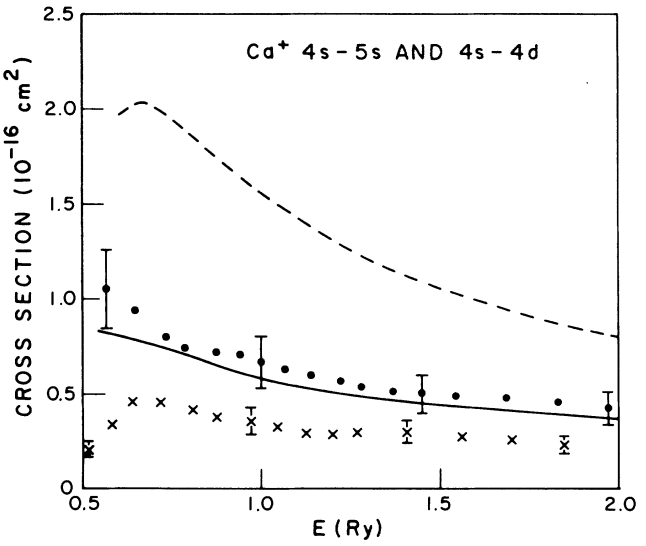

FIG. 6. Emission cross sections (in 10^{-16} cm^2) for excitation of the 5s (5s-$4p_{3/2}$ decay) and 4d (4d-$4p_{3/2}$ decay) states of Ca^+. The emission cross sections for the 5s (——) and 4d (— — —) levels resulting from the CCV6 calculation are depicted. The experimental emission cross sections of the 5s (●) and 4d (×) states (Ref. 6) are also presented.

ment with experiment. Experience with calculations on other systems[33–35] suggests that increasing the number of states in the close-coupling expansion will result in smaller cross sections for exciting the $4p$ as well as the $5s$, $4d$, and $5p$ states. While these additional states can potentially cascade into the $4p$ level, other decay routes are possible. Unlike excitations to the $4d$ and $5s$ levels the branching ratio for an eventual cascade into the $4p$ state for these higher states will be less than unity.

VII. CONCLUSIONS

We have performed extensive close-coupling, unitarized Coulomb-Born, and unitarized distorted-wave calculations of the electron-impact excitation of the valence electron in Ca^+. Theoretical six-state close-coupling results for the emission cross section and polarization associated with the $4s$-$4p_{3/2}$ excitation are in good agreement with experiment if the effects of cascading are ignored. When the calculated cross sections for excitation of the $5s$, $4d$, and $5p$ levels are used to estimate the effects of cascading, the theoretical emission cross section exceeds the experimental cross section by about 20% at incident energies just above the $5p$ threshold. It is apparent that our calculated cross sections for excitation of these higher states (especially $4d$) are too large, and that a more extensive calculation involving coupling with higher-lying states (especially $4f$) will be needed to properly account for cascade effects.

Comparison of our calculations with the results of earlier theoretical work reveals that the effects of core polarization and dielectronic polarization on the valence and continuum electron work to significantly reduce the magnitude of both the $4s$-$4p$ and $4s$-$3d$ excitation cross sections. This comparison is strongly reinforced by comparison with the results of a recent six-state close-coupling calculation,[7] in which polarization effects were not included. Such polarization effects should be large in all alkalilike systems that have an underlying core with a moderately large dipole polarizability. These effects partially explain the large discrepancy between experiment[36] and theory[8] for the $6s$-$6p$ excitation in Ba^+.

Continuum-coupling effects are also seen to be quite significant. The fact that the distorted-wave and Coulomb-Born results for the $4s$-$4p$ excitation exceed the six-state close-coupling results by less than 20% near threshold would indicate that, for this transition, one can obtain reasonable estimates of coupling effects by simple unitarization of the K-matrix elements calculated from a perturbation approach. Nevertheless, coupling effects are still quite large, since we have found that the distorted-wave and Coulomb-Born cross sections without unitarization exceed the unitarized cross sections by a factor of at least 50% near threshold. Other authors[8,9] have also found that unitarized calculations give much smaller cross sections than nonunitarized calculations. In the case of the $4s$-$3d$ transition, the coupling effects are even stronger. For this transition both the unitarized Coulomb-Born and distorted-wave cross sections are much larger than those obtained from the six-state close-coupling calculation. In addition, these coupling effects persist to very high partial waves, and even for $L=20$, the perturbation approaches yield partial cross sections that exceed the close-coupling results by more than a factor of 2.

It is expected that polarization effects as well as continuum-coupling effects will disappear as the ionization stage is increased. This latter argument has been used to justify the use of the distorted-wave approximation for the calculation of electron-impact excitation of highly ionized systems. However, detailed comparisons between a perturbation approach and the close-coupling approximation as a function of ionization stage, such as that performed for hydrogenic systems,[37] is needed to determine when and if this hypothesis regarding coupling effects is valid for complex ions. As has been done in the present work, it is essential that such comparisons be made between calculations in which the same bound-state wave functions are employed; otherwise it is impossible to distinguish between coupling and structure effects.

In addition to the excitation of the valence electron in Ca^+ there is also interest in transitions involving excitation of the core electrons, e.g., $3p^6 4s$-$3p^5 4s\,3d$. These excitations are known to contribute significantly to the total ionization cross section of Ca^+, through a two-step process involving excitation followed by autoionization.[38] Both distorted-wave[39] and close-coupling calculations[26,40] have been performed on this transition; however, large discrepancies between experiment and theory exist. The results of the present calculation may shed some light on the difficulties associated with the calculation of these complicated inner-shell processes. First, all of the effects of polarization should be important in the $3p$-$3d$ excitation; however, the actual calculation of these effects will be more complicated because of the complexity of the final configuration. In addition, the coupling effects between the valence states are very strong in this ion, so the limited couplings that have been included in calculations to date are not nearly sufficient to obtain an accurate cross section. It appears that a very large calculation will be required to yield reliable $3p$-$3d$ excitation cross sections.

ACKNOWLEDGMENTS

This work has been supported by the United States Department of Energy (Office of Fusion Energy), under Contract No. DE-AI05-86ER53237 with the National Bureau of Standards (J.M. and D.W.N.), Contract No. DE-AC05-84OR21400 with Martin Marietta Energy Systems, Inc. (D.C.G.), and Contract No. DE-FG05-86ER53217 with Auburn University (M.S.P.). We wish to thank G. H. Dunn for a number of useful conversations regarding the experimental results, and we are grateful to J. W. Gallagher and the members of the Joint Institute for Laboratory Physics (JILA) Data Center for assistance with the digitizing of published graphical results. One of us (D.C.G.) acknowledges support from the JILA Visiting Fellows Program. The calculations performed in this work were done with the CDC Cyber 205 at the National Bureau of Standards, Gaithersburg, the Cray 1 computer at the Magnetic Fusion Energy center at Livermore, and the VAX 8600 at JILA.

*Permanent address: Department of Theoretical Physics, The Australian National University, GPO Box 4, Canberra ACT 2601, Australia.

†Permanent address: Department of Physics, Rollins College, Winter Park, FL 32789.

‡Quantum Physics Division, National Bureau of Standards, Boulder, CO, 80309-0440.

[1]P. O. Taylor and G. H. Dunn, Phys. Rev. A **8**, 2304 (1973).

[2]P. G. Burke and D. L. Moores, J. Phys. B **1**, 575 (1968).

[3]H. van Regemorter, Mon. Not. R. Astron. Soc. **121**, 213 (1960).

[4]A. Petrini, C. R. Acad. Sci. (Paris) **260**, 4929 (1965).

[5]A. N. Tripathi, K. C. Mathur, and S. K. Joshi, Phys. Rev. A **1**, 337 (1970).

[6]I. P. Zapesochnyi, V. A. Kel'man, A. I. Imre, A. I. Dashchenko, and F. F. Danch, Zh. Eksp. Teor. Fiz. **69**, 1948 (1975) [Sov. Phys.—JETP **42**, 989 (1976)].

[7]A. Z. Msezane, J. Phys. B **21**, L61 (1988). This paper appeared just as the present manuscript was being completed.

[8]A. Burgess and V. B. Sheorey, J. Phys. B **7**, 2403 (1974).

[9]J. V. Kennedy, V. P. Myerscough, and M. R. C. McDowell, J. Phys. B **11**, 1303 (1978).

[10]M. Chidichimo, J. Phys. B **14**, 4149 (1981).

[11]U. Öpik, Proc. Phys. Soc. **92**, 566 (1967).

[12]H.-J. Werner and W. Meyer, Phys. Rev. A **14**, 915 (1976).

[13]W. Müller, J. Flesch, and W. Meyer, J. Chem. Phys. **80**, 3297 (1984).

[14]C. Froese-Fischer, Comput. Phys. Commun. **14**, 145 (1978).

[15]S. Bashkin and J. O. Stoner, *Atomic Energy Levels and Grotrian Diagrams* (North-Holland, Amsterdam, 1975), Vol. 3.

[16]D. W. Norcross and M. J. Seaton, J. Phys. B **9**, 2983 (1976).

[17]P. Hafner and W. H. E. Schwartz, J. Phys. B **11**, 2975 (1978).

[18]B. Emmoth, M. Braun, J. Bromander, and I. Martinson, Phys. Scr. **12**, 220 (1975).

[19]W. H. Smith and H. V. Liszt, J. Opt. Soc. Am. **61**, 938 (1971).

[20]A. C. Gallagher, Phys. Rev. **157**, 24 (1967).

[21]T. Andersen, J. Desesquelles, K. A. Jessen, and G. Sorensen, J. Quant. Spectrosc. Radiat. Transfer **10**, 1143 (1970).

[22]F. H. K. Rambow and L. D. Schearer, Phys. Rev. A **14**, 1735 (1976).

[23]S. Hameed, A. Herzenberg, and M. G. James, J. Phys. B **1**, 822 (1968); S. Hameed, *ibid.* **5**, 746 (1972).

[24]C. Froese-Fischer, Can. J. Phys. **54**, 1465 (1976).

[25]This program is unpublished. Recent references are *Atoms in Astrophysics*, edited by P. G. Burke and W. Eissner (Plenum, New York, 1983); H. Nussbaumer and P. J. Storey, in *ibid.*

[26]M. S. Pindzola, C. Bottcher, and D. C. Griffin, J. Phys. B **20**, 3535 (1987).

[27]M. A. Crees, M. J. Seaton, and P. M. H. Wilson, Comput. Phys. Commun. **15**, 23 (1978).

[28]A. Burgess, J. Phys. B **7**, L364 (1974).

[29]V. M. Burke and M. J. Seaton, J. Phys. B **19**, L257 (1986).

[30]I. C. Percival and M. J. Seaton, Philos. Trans. R. Soc. London, Ser. A **251**, 113 (1958).

[31]H. E. Saraph, J. Phys. B **3**, 952 (1970).

[32]J. Mitroy, Phys. Rev. A **37**, 649 (1988).

[33]M. A. Hayes, D. W. Norcross, J. B. Mann, and W. D. Robb, J. Phys. B **11**, L429 (1977).

[34]J. Mitroy and D. W. Norcross, Phys. Rev. A **37**, 3755 (1988).

[35]R. J. W. Henry, Phys. Rep. **68**, 1 (1981).

[36]D. H. Crandall, P. O. Taylor, and G. H. Dunn, Phys. Rev. A **10**, 141 (1974).

[37]M. A. Hayes and M. J. Seaton, J. Phys. B **10**, L573 (1977).

[38]B. Peart and K. T. Dolder, J. Phys. B **8**, 56 (1975).

[39]D. C. Griffin, M. S. Pindzola, and C. Bottcher, J. Phys. B **17**, 3183 (1984).

[40]P. G. Burke, A. E. Kingston, and A. Thompson, J. Phys. B **16**, L385 (1983).